Nanoscale

ROYAL SOCIETY OF CHEMISTRY

COMMUNICATION

View Article Online
View Journal | View Issue

Cite this: *Nanoscale*, 2024, **16**, 3422

Received 26th December 2023,
Accepted 13th January 2024

DOI: 10.1039/d3nr06597a

rsc.li/nanoscale

Bacterially synthesized superfine tellurium nanoneedles as an antibacterial and solar-thermal still for efficient purification of polluted water†

Yu Wang, Zhongming Huang, Yijian Gao, Jie Yu, Jie Zhang, Xiliang Li, Yuliang Yang, Qi Zhao and Shengliang Li *

Bacterial biosynthesis of nanomaterials has several advantages (*e.g.*, reduced energy inputs, lower cost, negligible environmental pollution) compared with traditional approaches. Various nanomaterials have been produced by bacteria. However, reports on using the bacterial biosynthesis of nanomaterials for applications with solar-thermal agents are scarce due to their narrow optical absorption. Herein, for the first time, we proposed a bacterial biosynthesis of broad-absorbing tellurium nanoneedles and demonstrated their effectiveness for solar-thermal evaporation and antibacterial applications. By simple biosynthesis within bacteria (*Shewanella oneidensis* MR-1), tellurium nanoneedles achieved a superfine configuration with a length-to-diameter ratio of nearly 20 and broad-spectrum absorbance. After integrating tellurium nanoneedles into a porous polyvinyl-alcohol scaffold, a solar-thermal still named TSAS-3 realized a high evaporation rate of 2.25 kg m^{-2} h^{-1} and solar-thermal conversion efficiency of 81% upon 1-Sun illumination. Based on these unique properties, the scaffold displayed good performances in seawater desalination, multiple wastewater treatment, and antibacterial applications. This work provides a simple and feasible strategy for the use of microbial-synthesized nanomaterials in solar-driven water purification and antibacterial applications.

College of Pharmaceutical Sciences, Soochow University, Suzhou, 215123, P. R. China. E-mail: lishengliang@suda.edu.cn

†Electronic supplementary information (ESI) available. See DOI: **https://doi.org/10.1039/d3nr06597a**

Shengliang Li

Shengliang Li is a Professor in the College of Pharmaceutical Sciences at Soochow University. He received his doctorate from Sun Yat-Sen University and National Center for Nanoscience and Technology. He spent 4 years undertaking postdoctoral research at the Institute of Chemistry within the Chinese Academy of Sciences, University of Massachusetts Medical School, and Houston Methodist Research Institute. He was a Senior Research Associate at the City University of Hong Kong (2018–2021). His research interests focus on molecular design, nanotechnology engineering, and mechanistic studies of photoactive materials for enabling applications in disease theranostics, chemical biology, and environmental health.

Introduction

In spite of 72% of the Earth's surface being covered by water, freshwater resources that humans can use directly are only 0.3% of this total. Moreover, the growing population and man-made pollution has placed the world into an emergency water-shortage scenario.[1] The *United Nations World Water Development Report 2023* predicted that 6-billion people will be facing water scarcity by 2050.[2,3] Hence, the shortage of freshwater resources is a major waiting and urgent unsolved problem. Seawater desalination is considered a choice for alleviating the escalating global freshwater scarcity.[4–6] Many researchers have developed engineering methods (*e.g.*, reverse osmosis, distillation, electrodialysis) to try to solve this issue.[7–11] However, the technologies usually require large amounts of input (electrical or chemical energy), which increases the carbon load and places an enormous burden upon the environment.[12–14] Thus, environmentally friendly and energy-free methods are needed urgently.[15]

Solar-thermal water evaporation is an emerging technology that utilizes photothermal materials to convert solar energy into heat energy for generation of interfacial water evaporation.[16–18] Solar-driven water evaporation uses only clean fuel solar energy without input from any other type of energy. Thus, it has been used widely in seawater desalination, sewage purification, electric-energy generation, photothermal

catalysis, and sterilization.[19] Solar-thermal materials are key components in the system for solar-driven water evaporation.[20,21] They have achieved considerable development in recent years, mainly based on metallic nanostructures, inorganic semiconductor materials, polymeric materials, and carbo-based materials.[22–32] Metals such as gold (Au), silver (Ag), aluminum (Al), copper (Cu) and palladium (Pd) in the form of nanoparticles or composites have a local surface plasmon resonance effect to produce solar-thermal conversion. Thus, they have been applied widely in solar-driven water evaporation.[33] However, most of these solar-thermal materials often require complicated chemical synthesis and nanofabrication. This can induce excessive energy consumption (*e.g.*, 120–600 °C and ~1000 bar) and environmental pollution due to toxic organic solvents (*e.g.*, PhMe and *n*-hexane).[34] Thus, developing and designing an easier, more effective solution free of chemosynthesis for the synthesis of solar-thermal materials is desired.[35]

Bacteria, along with various enzymes, non-enzyme proteins, peptides, and components of electron-transport species, can achieve the biosynthesis of nanomaterials without requiring harsh conditions or toxic solvents. Hence, they have become potential candidates in nanomaterial synthesis to address challenges in chemical and physical syntheses.[36–38] First, biosynthesized nanomaterials can be produced in normal culture media or buffered solutions free from the toxic contamination of byproducts. Second, biosynthesis does not necessitate additional stabilizing agents, thereby avoiding environmental pollution and possible biosafety issues. Third, synthesizing nanoparticles using bacteria has the advantages of high yield and controlled morphologies.[39–41] Various nanomaterials, mainly nanoparticles based on noble metals (*e.g.*, Au, Ag, Pt, Pd) or transition metals (*e.g.* Mn, Fe, Cu, Se), have been prepared by bacterial biosynthesis.[42–45] However, few reports have focused on the bacterial biosynthesis of nanomaterials with broadband absorption, especially covering full-spectrum with high efficiency for photothermal conversion.[46] Therefore, exploring high-performance nanomaterials *via* simple biosynthesis is a rational approach.

In this work, we first developed a facial and high-yield biosynthesis of superfine tellurium nanoneedles (Te NDs) within bacteria and applied them for solar-thermal still-based water purification and antibacterial applications. *Via* bacterial biosynthesis, Te NDs with a length-to-diameter ratio of nearly 20 were demonstrated to have full-spectrum absorbance and solar-thermal performances. By integrating Te NDs into a porous polyvinyl alcohol (PVA) scaffold, the solar-thermal still TSAS-3 achieved a high evaporation rate (2.25 kg m^{-2} h^{-1}) and solar-thermal conversion efficiency (81%) upon illumination (1 Sun light). These data were comparable with those of most reported solar-thermal materials produced by chemosynthesis. With these merits, the scaffold displayed good performance in seawater desalination and multiple wastewater treatment, with nearly 100% bacteria-killing performances. This work demonstrates the feasibility of microbial biosynthesis in the development of solar-thermal nanomaterials, and also identifies their potential in solar-driven water purification and antibacterial applications.

Results and discussion

Synthesis and characterization of Te@SOM

Bioactive molecules and proteins present within microorganisms can reduce high-valence metal ions to low-valence states, which provides a pathway of *in situ* biosynthesis to obtain Te NDs (Fig. 1A). After co-incubation with sodium tellurite (Na_2TeO_3), a mixture of *Shewanella oneidensis* MR-1 and Na_2TeO_3 turned black, indicating generation of an absorber (Fig. S1†). The absorbance of the *Shewanella oneidensis* MR-1 dispersion in the range 400–1300 nm showed an obvious improvement in a concentration-dependent manner (Fig. 1B). The improvement in absorbance of the bacterial dispersion was also demonstrated upon co-incubation in a time-dependent manner. The co-incubated sample after 6 h could reach a plateau in absorbance improvement (Fig. 1C). These results demonstrated that broad-absorbing Te NDs could be biosynthesized by *S. oneidensis* MR-1. To further verify the biosynthesis of Te NDs, a solution of *S. oneidensis* MR-1 was inactivated and then incubated with Na_2TeO_3. There was no significant change in color in identical synthetic conditions (Fig. S2†), which indicated that living bacterial cells were the primary factors during NDs the biosynthesis. Then, the biosynthesis of Te NDs in *S. oneidensis* MR-1 was imaged by TEM and elemental mapping. Vimineous Te NDs of diameter 100–150 nm were mainly precipitated within *S. oneidensis* MR-1, whereas outer bacteria had no traces of Te NDs (Fig. 1D). SEM images of *S. oneidensis* MR-1 with Te NDs biosynthesis revealed Te NDs to be distributed almost entirely within bacteria (Fig. 1E). As a control, untreated bacteria showed no Te NDs in bacterial cells (Fig. S3†). To verify these results, the supernatant and *S. oneidensis* MR-1 with Te NDs biosynthesis were separated by simple centrifugation. Obvious color and absorbance were absent in the supernatant, whereas the resuspended bacterial precipitate exhibited the same typical color and absorbance of the original mixed solution (Fig. S4†). These results indicated that Te NDs were mainly synthesized *in situ* within *S. oneidensis* MR-1 *via* biosynthesis by living bacteria. The similar biosynthesis of Te NDs was successfully realized in other microbes including *Escherichia coli*, *Pseudomonas aeruginosa*, and *Staphylococcus aureus* (Fig. S5†).

In order to examine the fine structures of Te NDs biosynthesized by *S. oneidensis* MR-1, the Te NDs were separated from the bacterial cells *via* a typical replacement method, that was, resuspending the bacterial precipitate in hexadecyl trimethyl ammonium bromide (CTAB) and ultrasonication. As the TEM image is shown in Fig. 1F, the biosynthesized Te NDs have a superfine appearance with a length-to-diameter ratio of nearly 20. Besides, the separated Te NDs show a broad absorbance in the visible and near-infrared region in a concentration-dependent manner (Fig. 1G). For the convenience of a subsequent application, the Te NDs covered by bacterial debris were

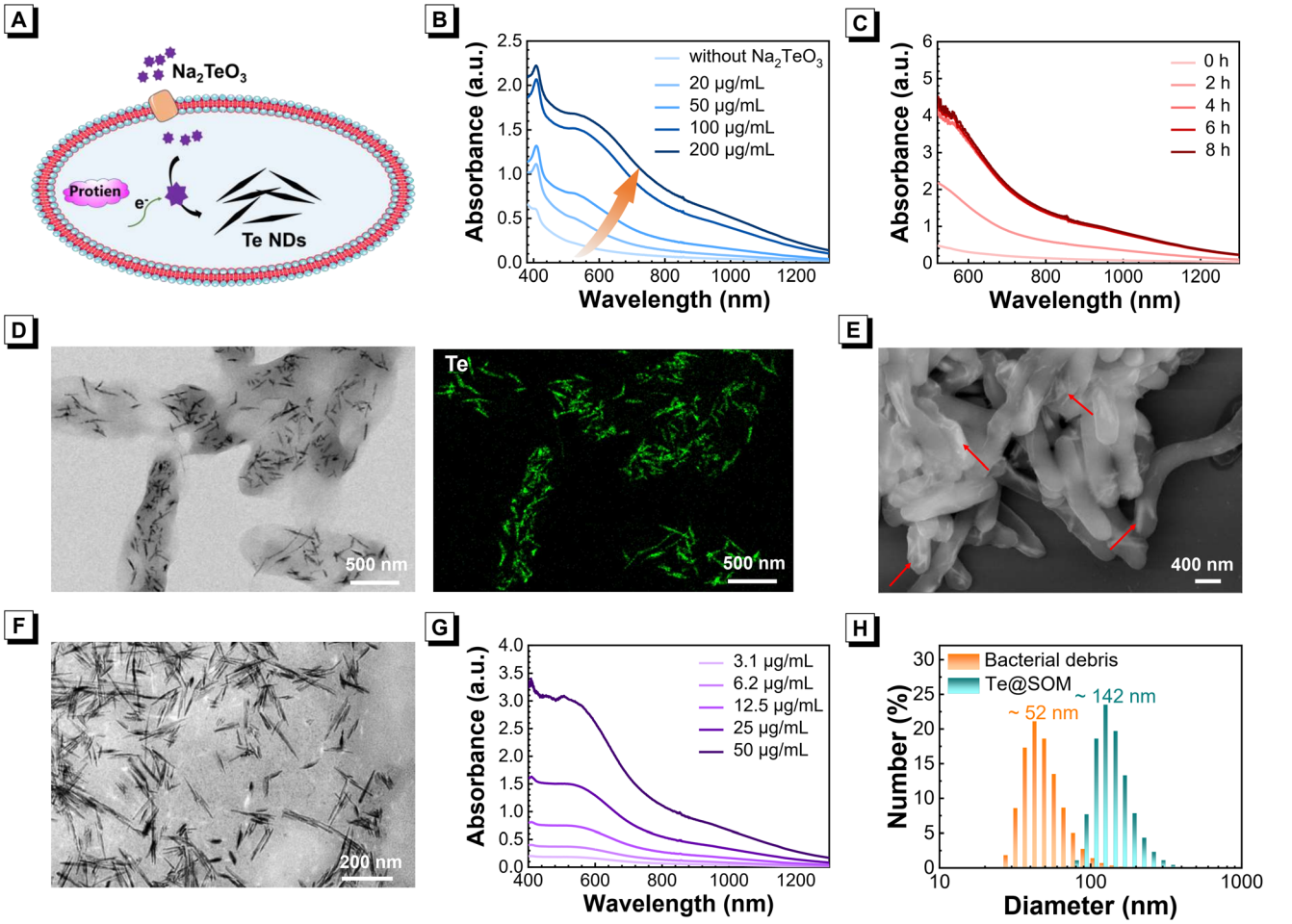

Fig. 1 (A) Biosynthesis of Te NDs by *S. oneidensis* MR-1 (schematic). (B) Absorption spectra of a mixture of *S. oneidensis* MR-1 and various concentrations of Na_2TeO_3. (C) Absorption spectra of a mixture of *S. oneidensis* MR-1 and Na_2TeO_3 as a function of reaction time. (D) TEM image and the corresponding elemental mapping of tellurium of *S. oneidensis* MR-1 with Te NDs biosynthesis. (E) SEM image of *S. oneidensis* MR-1 with Te NDs biosynthesis. (F) TEM image of Te NDs separated from bacteria. (G) Absorption spectra of Te NDs at various concentrations. (H) Diameter of *S. oneidensis* MR-1 debris and Te@SOM detected by DLS.

further obtained by ultrasonication and marked as Te@SOM. As shown in Fig. 1H, the size of Te@SOM was further measured to be 142 nm, which agrees with the TEM image in Fig. 1D. The negative potential of Te@SOM demonstrated that the surface of Te NDs is attached to the bacterial debris (Fig. S6†). Furthermore, the size stability of Te@SOM is investigated and demonstrated that the size and relevant polydispersity index (PDI) value of Te@SOM remains relatively high stability within 7-day storage (Fig. S7†). Therefore, the Te NDs synthesized in the interior of *S. oneidensis* MR-1 were successfully separated and their broad absorption capability was also demonstrated.

Preparation and characterization of TSAS

To achieve an afloat scaffold (TSAS) with good water transport and low thermal loss, the resulting Te@SOM was *in situ* doped into PVA for further co-gelation. After freezing-drying, TSAS with various loadings of nanomaterials (weight ratio of PVA : Te NDs of 1 : 1.25 (TSAS-1); 1 : 2.5 (TSAS-2); 1 : 3.75 (TSAS-3); 1 : 5 (TSAS-4); 1 : 7.5 (TSAS-5)) were fabricated (Fig. S8†). TSAS-3 displayed good optical absorption in the range 300–2500 nm, whereas a pristine PVA scaffold without Te NDs doping had extremely low absorption in visible and infrared regions (Fig. 2A). SEM images (Fig. 2B and C) indicated that TSAS-3 exhibited a loose and porous microstructure with an obvious channel, which was similar to the pristine PVA scaffold. The abundant Te element on the surface of TSAS-3 shown by elemental mapping corresponded with the SEM image, indicating efficient doping of Te@SOM. Next, the solar-thermal conversion of TSAS-3 was investigated by illumination (1 Sun) for 2 min. As shown in Fig. 2D, the temperature of TSAS rose from 22 °C to 60 °C within 2 min of illumination. However, the pristine PVA scaffold without Te NDs doping had a slight temperature change of 8 °C. These results demonstrated that TSAS-3 had good solar-thermal conversion under 1-Sun illumination. The solar-thermal stability of TSAS-3 was also indicated by a solar-thermal experiment of five cycles

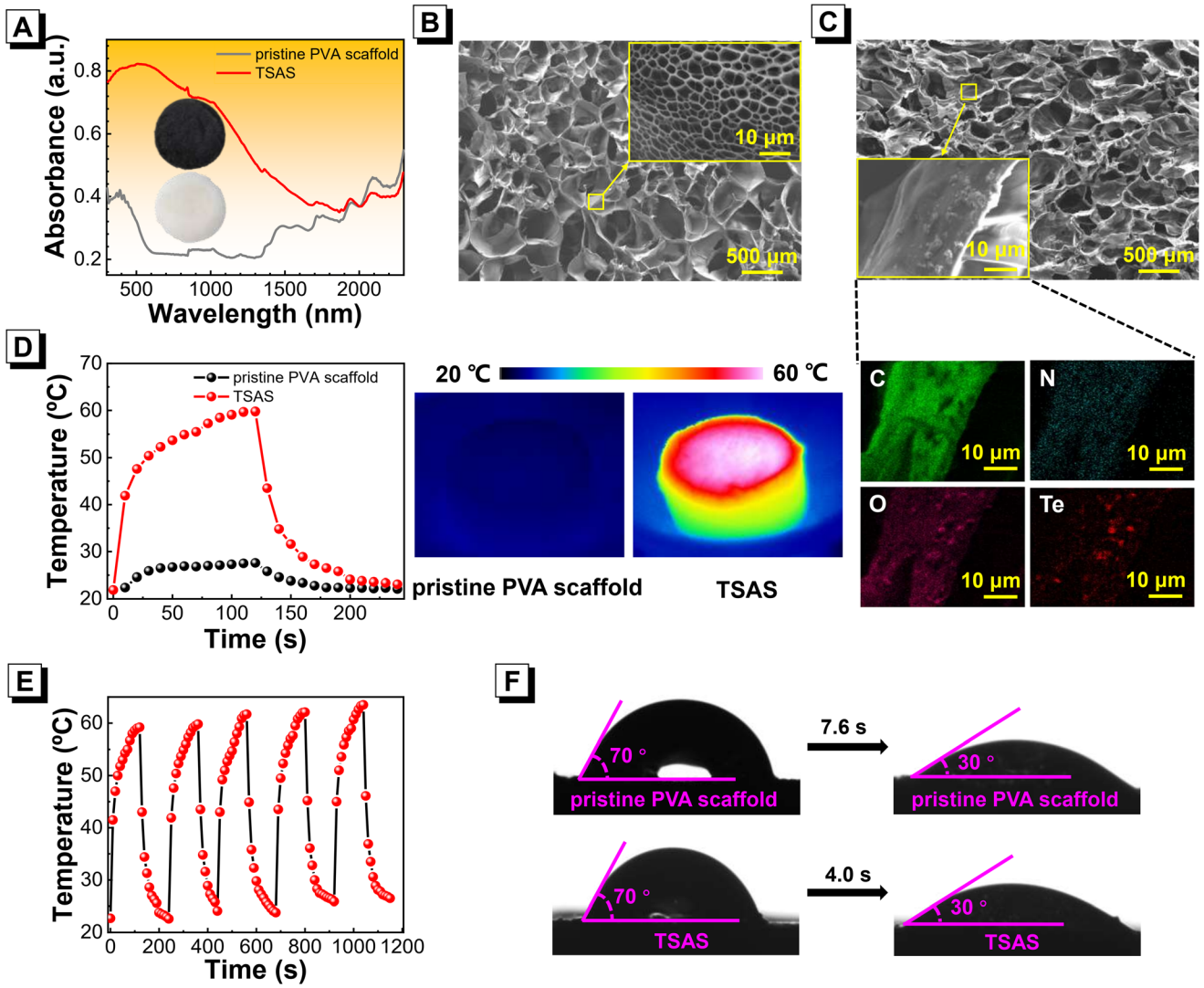

Fig. 2 (A) Absorption spectra of a pristine PVA scaffold and TSAS-3 (insets are the photographs of two scaffolds). SEM images and elemental mapping of a pristine PVA scaffold (B) and TSAS-3 (C). (D) Solar-thermal curves and thermal images of pristine PVA and TSAS-3 under 1-Sun illumination for 2 min. (E) Solar-thermal curves of TSAS-3 upon five cycles of 1-Sun illumination. (F) Water contact angle of the pristine PVA scaffold and TASA-3 at different times.

(Fig. 2E). To evaluate the wettability and water-transport performances of TSAS-3, the water contact angle at various times of water contact with the scaffold was measured. As shown in Fig. 2F, the pristine PVA scaffold and TSAS-3 had a water contact angle of 70°, suggesting the relatively good wettability of the TSAS. After contact with water, a water contact angle of 40° for TSAS-3 was achieved within 4 s of contact, whereas that of the pristine PVA scaffold required 7.6 s. These data demonstrated that TSAS with Te@SOM doping had an enhanced water-transport performance. These results indicated that TSAS had a high ability for solar-thermal conversion under 1-Sun illumination with good water-transport performance.

Solar-driven water evaporation

Next, the solar-thermal performances of TSAS floated in water were measured under 1-Sun illumination. As shown in Fig. 3A, the local temperature of TSAS reached up to 40.7 °C after 10 min of illumination of 1 Sun, whereas the pristine PVA scaffold had a slight temperature increase under an identical condition. The solar-thermal performance of TSAS was also demonstrated by infrared thermal imaging (Fig. 3B). Moreover, the solar-thermal performances of TSAS-3 retained good stability after five solar-photothermal cycles (Fig. S9†). Due to this efficient solar-thermal performance, the generation of interfacial water steam of TSAS was demonstrated further. As shown in Fig. 3C, upon 2-Sun illumination, rapid generation of steam was observed in a short time of irradiation when the TSAS scaffold floated in water, indicating the feasible water-evaporation capability of the scaffold. Thus, next we evaluated the detailed water-evaporation performances of TSAS-1 to TSAS-5 with various doping ratios of Te@SOM. The mass loss of water upon floatation of the TSAS scaffold was monitored as

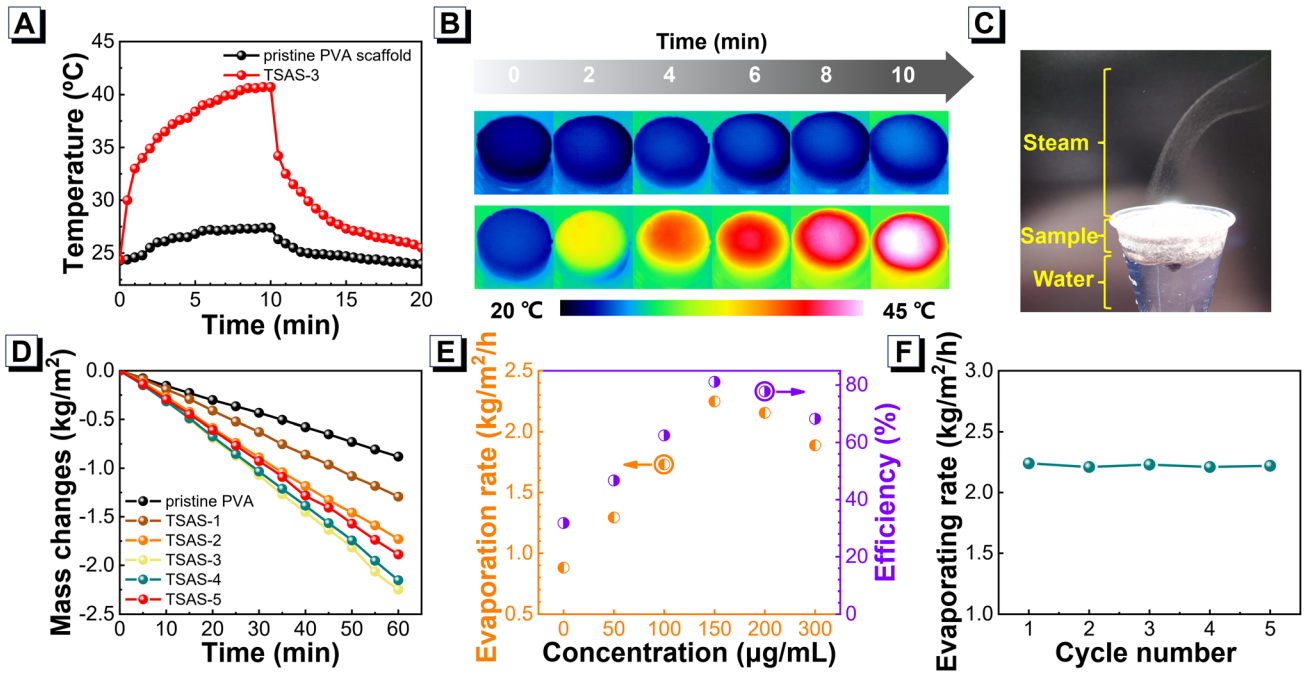

Fig. 3 (A) Temperature curves of different scaffolds floated in water under 10 min of 1-Sun illumination. (B) Thermal imaging of the corresponding scaffolds floated in water as a function of 1-Sun illumination. (C) Steam generation of TSAS-3 under 2-Sun illumination. (D) Mass changes of TSAS-1 to TSAS-5 upon 1-Sun illumination. (E) Evaporation rates and solar energy efficiencies of various TSAS types. (F) Stability characterization of TSAS-3 within five cycles of 1-Sun illumination (each cycle of Sun illumination lasted for 1 h).

a function of illumination duration under 1-Sun illumination (Fig. 3D). All water samples after TSAS treatments exhibited obvious mass loss, and the rate of water evaporation had a typical Te@SOM concentration-dependent profile. TSAS-3 with Te@SOM doping of 150 μg mL^{-1} achieved the highest water-evaporation rate (2.25 kg m^{-2} h^{-1}) with a relatively high solar-thermal conversion efficiency (81%) (Fig. 3E). Moreover, TSAS-3 could realize a water-evaporation rate of 4.16 and 6.76 kg m^{-2} h^{-1} upon illumination of 2 Sun and 3 Sun, respectively (Fig. S10†). The relatively high stability of TSAS-3 was shown by the experiment of five cycles of water evaporation (Fig. 3F). There were almost no significant changes or Te NDs leakage on TSAS-3 after soaking in water for 2 weeks (Fig. S11†). These results illustrated the high performance of water evaporation and good stability of TSAS-3.

Solar-driven water purification

In consideration of its good water-evaporation performance, the practical applications of TSAS-3 for water purification and antibacterial applications were explored. Seawater desalination was undertaken *via* solar-photothermal seawater vaporization and vapor-collection devices (Fig. S12†). As shown in Fig. 4A, after solar evaporation, orders-of-magnitude reduction of ion concentration (Na^+, Ca^{2+}, K^+, and Mg^{2+}) in seawater was achieved, and a removal efficiency of ~99.9% could meet the requirements of the WHO. Moreover, TSAS-3 was used to deionize wastewater with heavy metals *via* solar evaporation. All heavy-metal ions (Fe^{3+}, Co^{2+}, Hg^{2+}, Cu^{2+}, Ag^+, Cd^{2+}, Ni^{2+}, Pb^{2+}) in sewage were wiped out, with removal efficiency of >99.8% being noted (Fig. 4B). The residual level of heavy-metal ions in wastewater was much lower than the WHO standard for drinking water, thereby revealing the high-performance water purification of TSAS-3 *via* solar-driven water evaporation. Wastewater with toxic dye was also treated with solar-driven water evaporation of TSAS-3. As shown in Fig. 4C, the color of methylene blue (MB)-simulated dyestuff wastewater became transparent after solar-driven water evaporation by TSAS-3. UV-vis-NIR absorption further demonstrated that the typical absorption peak of MB dye was almost completely wiped out. These results indicated the good water-purification performances of the TSAS scaffold.

Microbial pollution is an important challenge in practical water purification. Next, we evaluated the microbial-removal capability of TSAS-3. Water containing 10^8 CFU mL^{-1} of Gram-negative (*Escherichia coli*) and Gram-positive (*Staphylococcus aureus*) bacteria was treated with TSAS-3 and 1-Sun illumination, respectively. The plate-counting method was performed to determine the residual cell concentration. As shown in Fig. 4D, after solar-driven treatment by TSAS-3, a removal efficiency of nearly 100% was achieved in *E. coli*- and *S. aureus*-polluted water. Thus, TSAS-3 displayed a good microbial-removal capability. To further demonstrate the practical potential of our method, the antibacterial performance of TSAS-3 was evaluated under 1-Sun illumination based on bacterial-inhibition zones. As shown in Fig. 4E, upon 1-Sun illumination, TSAS-3 had an obvious antibacterial effect. The bacterial-

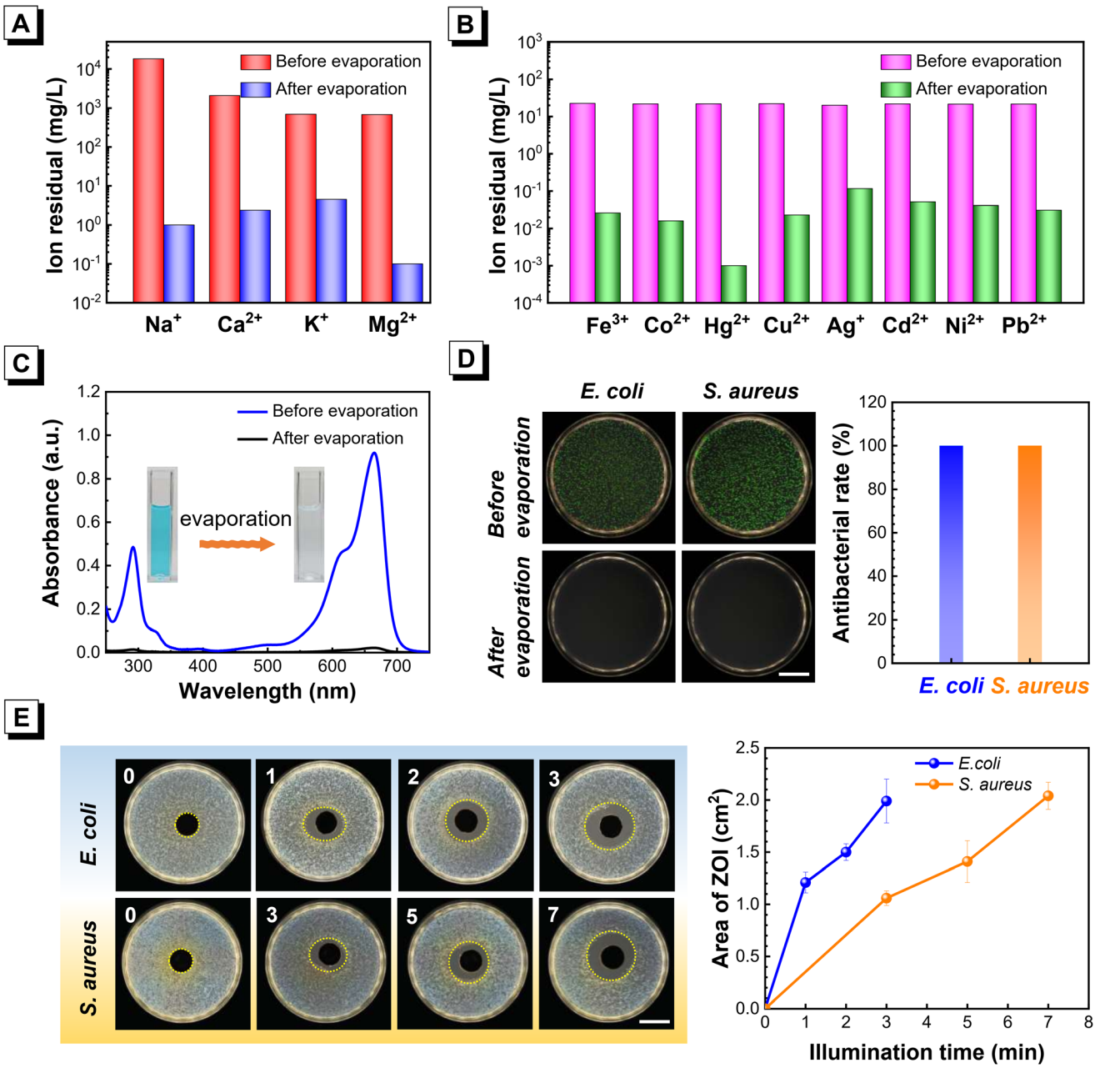

Fig. 4 (A) Metal-ion residues in seawater before and after solar-driven water evaporation by TSAS-3. (B) Residues of heavy-metal-ion residual in wastewater before and after solar-driven evaporation. (C) Absorption spectra of MB-simulated dyestuff wastewater before and after purification. The inset shows photographs of dyestuff wastewater before and after treatment. (D) Images and statistical analyses of colonies of *E. coli* and *S. aureus* before and after TSAS-3 treatment (scale bar: 25 mm). (E) Inhibition zones of *E. coli* and *S. aureus* upon different illumination times (scale bar: 25 mm).

inhibition zone broadened gradually with an increasing duration of irradiation, which demonstrated that the TSAS scaffold could realize efficient bacterial killing using 1-Sun illumination.

Conclusions

We described a simple and high-yield biosynthesis of superfine Te NDs within bacteria with full-spectrum solar absorption. Using this method, we developed a solar-thermal still by integration of Te NDs into a porous PVA scaffold. The solar-thermal still TSAS-3 exhibited superior photothermal conversion and photothermal stability upon 1-Sun illumination. An efficient solar-driven water-evaporation rate of 2.25 kg m^{-2} h^{-1} under 1-Sun illumination (1.0 kW m^{-2}) and high solar-thermal conversion efficiency of 81% were documented, which are comparable with most reported solar-thermal materials produced by chemosynthesis. Furthermore, the TSAS-3 still was

utilized to purify natural seawater and wastewater polluted with heavy metals, dye, or microorganisms. It achieved a high purification efficiency that could meet the WHO standards of potable water. The TSAS-3 still achieved nearly 100% bacteria-killing performance on the surface of microbes. This encouraging performance demonstrated the feasibility of microbial biosynthesis in the development of solar-thermal materials, and offers a way for solar-driven water-treatment applications.

Author contributions

Shengliang Li conceived and supervised the project. Yu Wang, Zhongming Huang and Yijian Gao carried out experimental planning, material preparations and data analyses. Jie Yu and Jie Zhang undertook characterizations of materials. Qi Zhao assisted the antifungal assay. Xiliang Li and Yuliang Yang assisted with data presentation.

Conflicts of interest

There are no conflicts of interest to declare.

Acknowledgements

The work was supported financially by the National Natural Science Foundation of China (52173135, 22207024), Jiangsu Specially Appointed Professorship, Leading Talents of Innovation and Entrepreneurship of Gusu (ZXL2022496), and the Suzhou Science and Technology Program (SKY2022039). The authors also acknowledge the project funded by the Priority Academic Program Development of Jiangsu Higher Education Institutions.

References

1 C. He, Z. Liu, J. Wu, X. Pan, Z. Fang, J. Li and B. A. Bryan, *Nat. Commun.*, 2021, **12**, 4667.
2 C. Hou, Y. Wen, X. Liu and M. Dong, *J. Cleaner Prod.*, 2021, **278**, 123965.
3 K. Liu, W. Cao, D. Zhao, S. Liu and J. Liu, *Environ. Res. Lett.*, 2022, **17**, 104056.
4 Y. Kuang, C. Chen, S. He, E. M. Hitz, Y. Wang, W. Gan, R. Mi and L. Hu, *Adv. Mater.*, 2019, **31**, 1900498.
5 X. Liu, F. Chen, Y. Li, H. Jiang, D. D. Mishra, F. Yu, Z. Chen, C. Hu, Y. Chen, L. Qu and W. Zheng, *Adv. Mater.*, 2022, **34**, 2203137.
6 B. Anand, R. Shankar, S. Murugavelh, W. Rivera, K. Midhun Prasad and R. Nagarajan, *Renewable Sustainable Energy Rev.*, 2021, **141**, 110787.
7 F. E. Ahmed, R. Hashaikeh and N. Hilal, *Desalination*, 2020, **495**, 114659.
8 A. D. Khawaji, I. K. Kutubkhanah and J. M. Wie, *Desalination*, 2008, **221**, 47–69.
9 Z. Y. Wang, Y. J. Zhu, Y. Q. Chen, H. P. Yu and Z. C. Xiong, *Small*, 2023, **19**, 2206917.
10 S. He, C. Chen, Y. Kuang, R. Mi, Y. Liu, Y. Pei, W. Kong, W. Gan, H. Xie, E. Hitz, C. Jia, X. Chen, A. Gong, J. Liao, J. Li, Z. J. Ren, B. Yang, S. Das and L. Hu, *Energy Environ. Sci.*, 2019, **12**, 1558–1567.
11 X. Zhou, F. Zhao, Y. Guo, Y. Zhang and G. Yu, *Energy Environ. Sci.*, 2018, **11**, 1985–1992.
12 Q. Wang, L. Wang, S. Song, Y. Li, F. Jia, T. Feng and N. Hu, *Desalination*, 2022, **525**, 115483.
13 F. Li, N. Li, S. Wang, L. Qiao, L. Yu, P. Murto and X. Xu, *Adv. Funct. Mater.*, 2021, **31**, 2104464.
14 A. Bamasag, E. Almatrafi, T. Alqahtani, P. Phelan, M. Ullah, M. Mustakeem, M. Obaid and N. Ghaffour, *J. Cleaner Prod.*, 2023, **385**, 135737.
15 J. Kim, J. Hwang, S. Kim, S. H. Cho, H. Choi, H.-Y. Kim and Y. S. Lee, *Int. J. Pr. Eng. Man-GT*, 2021, **8**, 1347–1367.
16 F. Zhao, Y. Guo, X. Zhou, W. Shi and G. Yu, *Nat. Rev. Mater.*, 2020, **5**, 388–401.
17 L. Cui, P. Zhang, Y. Xiao, Y. Liang, H. Liang, Z. Cheng and L. Qu, *Adv. Mater.*, 2018, **30**, e1706805.
18 N. Xu, J. Li, C. Finnerty, Y. Song, L. Zhou, B. Zhu, P. Wang, B. Mi and J. Zhu, *Nat. Water*, 2023, **1**, 494–501.
19 X. Hao, H. Yao, P. Zhang, Q. Liao, K. Zhu, J. Chang, H. Cheng, J. Yuan and L. Qu, *Nat. Water*, 2023, **1**, 982–991.
20 X. Wu, G. Y. Chen, G. Owens, D. Chu and H. Xu, *Mater. Today. Energy*, 2019, **12**, 277–296.
21 W. Wu, Y. Xu, X. Ma, Z. Tian, C. Zhang, J. Han, X. Han, S. He, G. Duan and Y. Li, *Adv. Funct. Mater.*, 2023, 2302351.
22 W. Guan, Y. Guo and G. Yu, *Small*, 2021, **17**, 2007176.
23 H. Lu, W. Shi, F. Zhao, W. Zhang, P. Zhang, C. Zhao and G. Yu, *Adv. Funct. Mater.*, 2021, **31**, 2101036.
24 J. H. Zhang, P. F. Wang, Y. L. Chen, X. J. Mu, X. Y. Wang, S. Tanemura, J. H. Zhou and L. Miao, *Nanoscale*, 2022, **14**, 6949.
25 C. Li, H. Jiang, P. Liu, Y. Zhai, X. Yang, L. Gao and L. Jiang, *J. Am. Chem. Soc.*, 2022, **144**, 9472–9478.
26 C. H. Huang, J. X. Huang, Y. H. Chiao, C. M. Chang, W. S. Hung, S. J. Lue, C. F. Wang, C. C. Hu, K. R. Lee, H. H. Pan and J. Y. Lai, *Adv. Funct. Mater.*, 2021, **31**, 2010422.
27 Y. Li, Y. Shi, H. Wang, T. Liu, X. Zheng, S. Gao and J. Lu, *Carbon Energy*, 2023, e331.
28 Z. Huang, Y. H. Luo, W. Y. Geng, Y. Wan, S. Li and C. S. Lee, *Small Methods*, 2021, **5**, 2100036.
29 S. Tian, Z. Huang, J. Tan, X. Cui, Y. Xiao, Y. Wan, X. Li, Q. Zhao, S. Li and C.-S. Lee, *ACS Energy Lett.*, 2020, **5**, 2698–2705.
30 Z. Huang, S. Li, X. Cui, Y. Wan, Y. Xiao, S. Tian, H. Wang, X. Li, Q. Zhao and C.-S. Lee, *J. Mater. Chem. A*, 2020, **8**, 10742–10746.
31 L. F. Cu, P. F. Wang, H. N. Che, X. Gao, J. Chen, B. Liu and Y. H. Ao, *Water Res.*, 2023, **244**, 120514.
32 B. S. Zhang, H. M. Chen, Y. C. Huang, W.-M. Lau and D. Zhou, *Chem. Eng. J.*, 2023, **468**, 143689.

33 Y. Wang, H. Ma, J. Yu, J. Li, N. Xu, J. Zhu and L. Zhou, *Adv. Opt. Mater.*, 2023, 2201907.
34 Z. Bo, S. Mao, Z. J. Han, K. Cen, J. Chen and K. K. Ostrikov, *Chem. Soc. Rev.*, 2015, **44**, 2108–2121.
35 Z. Huang, Y. Liu, S. Li, C. S. Lee and X. H. Zhang, *Small Methods*, 2022, **6**, e2200835.
36 A. Rana, K. Yadav and S. Jagadevan, *J. Cleaner Prod.*, 2020, **272**, 122880.
37 T. R. Yu, G. M. Jiang, R. F. Gao, G. J. Chen, Y. J. Ren, J. Liu, H. C. van der Mei and H. J. Busscher, *Expert Opin. Drug Delivery*, 2020, **17**, 1151–1164.
38 G. F. Luo, W. H. Chen, X. Zeng and X. Z. Zhang, *Chem. Soc. Rev.*, 2021, **50**, 945–985.
39 Y. Y. Wu, C. Li, H. C. van der Mei, H. J. Busscher and Y. J. Ren, *Antibiotics*, 2021, **10**, 623.
40 L. Zou, F. Zhu, Z. E. Long and Y. Huang, *J. Nanobiotechnol.*, 2021, **19**, 120.
41 N. I. Hulkoti and T. C. Taranath, *Colloids Surf., B*, 2014, **121**, 474–483.
42 K. B. Narayanan and N. Sakthivel, *Adv. Colloid Interface Sci.*, 2010, **156**, 1–13.
43 Y. Choi and S. Y. Lee, *Nat. Rev. Chem.*, 2020, **4**, 638–656.
44 G. Grasso, D. Zane and R. Dragone, *Nanomaterials*, 2020, **10**, 11.
45 J. Jeevanandam, S. F. Kiew, S. Boakye-Ansah, S. Y. Lau, A. Barhoum, M. K. Danquah and J. Rodrigues, *Nanoscale*, 2022, **14**, 2534–2571.
46 J. L. Wang, Y. Kong, Z. Liu and H. Q. Wang, *Nano Energy*, 2023, **108**, 108115.